Investigation of Fade Mitigation Methods on Experimental FSO LEO-to-Ground Links

Cuong T. Nguyen*, Hoang D. Le*, Dimitar R. Kolev†, Alberto Carrasco-Casado†, Toshihiro Kubo-oka†, Hiroyuki Tsuji†, Morio Toyoshima†, and Anh T. Pham*

* Computer Communications Laboratory, The University of Aizu, Aizuwakamatsu 965-8580, Japan

† Wireless Networks Research Center, National Institute of Information and Communications Technology, Tokyo 184-8795, Japan

***Abstract*—In recent years, the standardization of free-space optics (FSO)-based low-earth orbit (LEO) satellite communication systems has aroused growing interest. This is thanks to the ability to provide high data rates and global coverage of the optical satellite systems. However, one of the key challenges lies in selecting effective techniques to combat channel fading and improve system reliability. To address this, current standards consider forward error correction (FEC) codes and/or interleaving at the physical layer, along with automatic repeat request (ARQ) protocols at the link layer. This work aims to investigate and compare the performance of various fade mitigation strategies, which aligns with current standardization efforts. In particular, we conduct both information-theoretic analysis and simulation for key link-layer performance metrics, i.e., frame loss probability (FLP), goodput, and average system delay. Through this study, we provide insightful discussions and practical design guidelines that benefit the development of reliable optical satellite systems.**

***Index Terms*—Free-space optics (FSO), LEO satellite, automatic repeat request (ARQ), forward error correction (FEC), interleaving.**

I. Introduction

In recent years, free-space optics (FSO) communication systems leveraging low-earth orbit (LEO) satellites have emerged as a promising architecture for future wireless networks, offering high data rates and global coverage [1]. To enhance the commercial interoperability and accelerate the development cycles, the standardization of FSO satellite systems has gained significant momentum, attracting growing interest from both academia and industry. In response, experimental recommendations/recommended standards have been introduced, including the Blue Book/Orange Book by the Consultative Committee for Space Data Systems (CCSDS) [2], [3] and the Optical Communication Terminal (OCT) standard by the Space Development Agency (SDA) [4]. It is important to note, however, that these recommendations/standards remain under active development and are expected to evolve in the coming years.

One of the key challenges in standardizing optical satellite systems lies in selecting effective fade mitigation techniques. Optical LEO-to-ground links are highly susceptible to signal fading, primarily due to atmospheric turbulence and pointing errors, which cause fluctuations in received power and compromise system reliability. To tackle this issue, an indispensable approach is forward error correction (FEC) codes, which have been considered in all current recommendations [2]–[4]. However, relying solely on FEC can be insufficient due to the burst errors that occur over the FSO channels. In particular, the coherence time of FSO satellite channels is significantly larger than the data rate, resulting in the same channel conditions spanning multiple bits. If deep fading occurs, many consecutive bits will be canceled, resulting in performance degradation.

To further enhance the system reliability, channel interleavers have been promoted to use alongside FEC codes [3]. The key idea of interleaving is to spread consecutive bits over different channel conditions, making burst errors appear as randomly distributed errors. This allows all errors to be corrected by using a proper FEC code. Another approach is the deployment of automatic repeat request (ARQ) at the link layer [4]. In this method, corrupted frames will be retransmitted, increasing the chance that these frames can be received successfully. These methods provide more robust options to combat the fading but introduce a longer latency as a trade-off. For the development of practical systems, it is essential to have a comprehensive understanding of these techniques to determine the most suitable approach for specific operational requirements. However, within the context of optical satellite systems, these methods have predominantly been examined separately [5]–[11], with no existing comparative analysis available in the literature.

Motivated by this gap, our work aims to investigate and compare the performance of various fade mitigation techniques. In particular, we conduct both information-theoretic analysis and simulations for three key link-layer performance metrics, i.e., frame loss probability (FLP), goodput, and average system delay. The evaluation also incorporates the experimental FSO LEO-to-ground data conducted by the National Institute of Information and Communications Technology (NICT), Japan [12]. Based on the results, we provide insightful discussions and practical design guidelines that benefit the development of reliable optical satellite systems. Specifically, this work seeks to answer two fundamental questions: *(1) What are the potential use cases of each technique?* and *(2) How can optimal parameters be selected for a given operational scenario?*

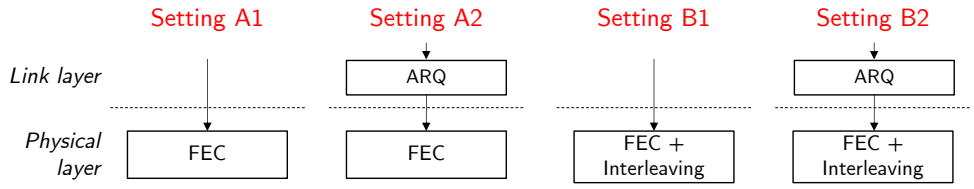

Fig. 1. Considered fade mitigation settings for the FSO satellite-to-ground channel.

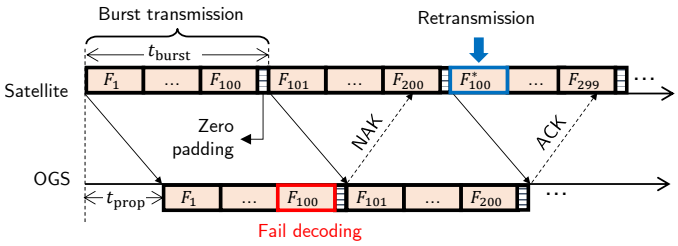

Fig. 2. Example of burst transmission in the considered systems.

II. System Model

This work investigates an FSO communication link from a LEO satellite to an optical ground station (OGS), focusing on the evaluation of fade mitigation strategies in alignment with current standardization efforts. As illustrated in Fig. 1, four configurations are examined, combining forward error correction (FEC) code and/or interleaving at the physical layer, and automatic repeat request (ARQ) protocols at the link layer. Note that in settings A1 and B1, ARQ is not enabled at the link layer.

We consider the time-slotted structure for data transmission, in which each fixed-duration slot contains a burst transmission of an integer number of link-layer frames. These frames will be acknowledged at once, as illustrated in Fig. 2. Zero padding can be appended to guarantee the burst duration. The number of frames in each burst is calculated as

$$n_{\text{frames}} = \left\lfloor \frac{t_{\text{burst}} M_{\text{s}} R_{\text{s}}}{k R_{\text{PHY}}} \right\rfloor, \tag{1}$$

where t_{burst} is the burst duration, M_{s} is the number of bits per symbol, R_{s} is the symbol rate, k is the link-layer frame size in bits, and R_{PHY} is the physical layer's code rate. In this work, we consider the on-off keying (OOK) modulation, resulting in $M_{\text{s}} = 1$. We assume that the feedback channel is error-free for the sake of simplicity. In the case of ARQ, frames that were received unsuccessfully will be retransmitted in the next burst. In the case of interleaving, since all interleaved data must be received before decoding, the burst duration will equal the interleaving time.

The received symbol at i-th symbol duration is given as

$$y[i] = h[i]\, x[i] + n[i], \tag{2}$$

where $x[i] \in \{x_0 = 0, x_1 = 2P_{\text{t}}\}$ is the OOK-modulated symbol, P_{t} is the average transmitted optical power, $h[i]$ is the channel coeffcient, $n[i]$ is zero-mean additive white Gaussian noise (AWGN) with variance σ_{n}^2, which is nomalized to unity for the sake of analysis. The channel coefficient $h[i]$ is taken from the normalized data of the Small Optical TrAnsponder (SOTA) experiment conducted by NICT. In this experiment, data is gathered from a 1550-nm downlink FSO channel between SOTA, which onboards a microsatellite, and a 5-cm receiver accommodated at the OGS. More details on the experimental setups can be found in [12], [13]. It is worth noting that the sampling rate of the data, f_{s}, is 20 kHz, which may be smaller than the considered symbol rate R_{s}. Threfore, we assume that the fading coefficient $h[i]$ is blockwise for $T_{\text{B}} = t_{\text{f}}/t_{\text{s}}$ consecutive symbols, where $t_{\text{f}} = 1/f_{\text{s}}$ is the channel sampling time and $t_{\text{b}} = 1/R_{\text{s}}$ is the symbol duration.

Finally, the instantaneous signal-to-noise ratio (SNR) is defined as [14]

$$\gamma = \frac{2P_{\text{t}}^2 h^2}{\sigma_{\text{n}}^2} = 2P_{\text{t}}^2 h^2. \tag{3}$$

From that, we also define the average SNR as the received SNR when there is no fading, i.e., $\overline{\gamma} = 2P_{\text{t}}^2$ [15].

III. Information-Theoretic Analysis

Aside from simulations, this work also presents an information-theoretic analysis of the considered link-layer performance metrics, namely FLP, goodput, and average system delay. Definitions of them and the analysis will be discussed in this section.

A. Frame loss probability

FLP denotes the probability that a link-layer frame can not be received successfully and can be computed as [16]

$$\text{FLP}_{\mathcal{X}_d} = \left(P_{\text{out},\,\mathcal{X}}\right)^M, \tag{4}$$

where $\mathcal{X} \in \{\text{A}, \text{B}\}$ and $d \in \{1, 2\}$ are used to denote the corresponded setting, $P_{\text{out},\,\mathcal{X}}$ is the outage probability at the physical layer of setting $\mathcal{X}_d$, M is the maximum number of ARQ rounds ($M = 1$ in case ARQ is not enabled).

As for settings A_d, it can assume that all symbols created from a frame experience the same fading coefficient due to the slow-varying property of the FSO channel compared to the symbol duration [1]. As a result, the outage event of settings A_d occurs when the instantaneous capacity is less than the transmission rate R, or [14]

$$P_{\text{out},\,\text{A}}(R) = \Pr\left[\mathcal{C}(h, \overline{\gamma}) < R\right], \tag{5}$$

[1]For example, the symbol duration is 1 nanosecond given the symbol rate is 1 giga symbol per second (GSps) while the coherence time of the LEO-to-ground channel is in the order of milliseconds (ms) [12].

where the transmission rate is computed as $R = k/L$ (bits per channel use), $L = \frac{k}{M_s R_{\text{PHY}}}$ is the number of symbols used to transmit k information bits [17]. Moreover, the channel capacity can be computed as [14]

$$\mathcal{C}\left(h_j, \overline{\gamma}\right) = \int_{-\infty}^{\infty} \sum_{x \in \{x_0, x_1\}} p_{Y|X}\left(y|x\right) P_X\left(x\right) \log_2 \left[\frac{p_{Y|X}\left(y|x\right)}{p_Y\left(y\right)}\right] \mathrm{d}y. \quad (6)$$

After a few steps of mathematical transformation, the channel capacity with OOK modulation can be derived as

$$\mathcal{C}\left(h, \overline{\gamma}\right) = \int_{-\infty}^{\infty} \frac{1}{\sqrt{2\pi}} \exp\left(-\frac{y^2}{2}\right) \log\left[\frac{2}{1 + \exp\left(2P_{\text{t}} h y - 2P_{\text{t}}^2 h^2\right)}\right] \mathrm{d}y. \quad (7)$$

Since $\mathcal{C}\left(\cdot\right)$ is monotonically increasing, we can rewrite (5) as

$$\begin{aligned} P_{\text{out, A}} &= \Pr\left[h < \mathcal{C}^{-1}\left(R_{\text{PHY}}, \overline{\gamma}\right)\right] \\ &= F_h\left[\mathcal{C}^{-1}\left(R_{\text{PHY}}, \overline{\gamma}\right)\right], \end{aligned} \quad (8)$$

where $F_h\left[\cdot\right]$ is the cumulative distribution function (CDF) of the channel coefficient h. The distribution of h is derived by curve-fitting the histogram of the data set, which will be presented in Section IV. To approximate the inverse function $\mathcal{C}^{-1}\left(\cdot\right)$, we utilize the fixed-point iteration method [18].

Regarding settings with interleaving (B_d), it is well-known that a channel with perfect interleaving can be modeled as a memoryless, stationary, and ergodic channel with independent and identically distributed (i.i.d.) fading statistics [19]. However, practical interleavers have limited time due to delay constraints or limited hardware resources. As in that case, it is observed that the outage event can still happen [20]. Therefore, in this work, we derive the equation for the outage probability given the finite time of the interleavers. To achieve that, we first divide the considered channel samples into n_{IL} interleaving groups. Particularly, $n_{\text{IL}} = \left\lfloor \frac{n_{\text{samples}}}{n_{\text{sIL}}} \right\rfloor$, n_{samples} is the number of considered samples, n_{sIL} is the number of samples per interleaving group and can be computed as $n_{\text{sIL}} = f_{\text{s}} \ell_{\text{IL}}$, and ℓ_{IL} is the interleaving time. The outage probability of systems B_d is written as

$$P_{\text{out, B}} = \frac{\Pr\left[\mathcal{C}_{\text{erg}}^{(i)} \leq R \mid i \in [1, n_{\text{IL}}]\right]}{n_{\text{IL}}}, \quad (9)$$

where $\mathcal{C}_{\text{erg}}^{(i)}$ is the ergodic capacity considering samples of the i-th interleaving group and can be calculated as

$$\mathcal{C}_{\text{erg}}^{(i)} = \frac{1}{n_{\text{sIL}}} \sum_{j=(i-1)n_{\text{sIL}}+1}^{in_{\text{sIL}}} \mathcal{C}\left(h_j, \overline{\gamma}\right). \quad (10)$$

B. Goodput

Goodput is defined as the average rate of successfully received data and can be expressed as [16]

$$\eta_{\mathcal{X}_d} = \frac{R\left(1 - \text{FLP}_{\mathcal{X}_d}\right)}{\overline{m}_{\mathcal{X}_d}}, \quad (11)$$

TABLE I
PHYSICAL CHARACTERISTICS OF THE CONSIDERED DATA SETS (μ, σ: THE MEAN AND VARIANCE OF THE LOG-NORMAL DISTRIBUTION).

#	SI	Coherence time	R^2, (μ, σ)
1	0.1140	0.55 ms	$0.9966\,(-0.057, 0.3228)$
2	0.2015	0.45 ms	$0.9898\,(-0.059, 0.4411)$
3	0.2927	0.55 ms	$0.9902\,(-0.08, 0.5587)$

where $\overline{m}_{\mathcal{X}_d}$ is the average number of ARQ rounds and can be derived as

$$\overline{m}_{\mathcal{X}_d} = M P_{\text{out, }\mathcal{X}}^{M} + \sum_{m=1}^{M} m\left(1 - P_{\text{out, }\mathcal{X}}\right) P_{\text{out, }\mathcal{X}}^{m-1}. \quad (12)$$

C. Average system delay

Next, we consider the average system delay, denoted as the average duration since a frame is transmitted until it is discarded or received successfully. The average system delay of the setting $\mathcal{X}_d$ is computed as

$$D_{\mathcal{X}_d} = M d_{\mathcal{X}} P_{\text{out, }\mathcal{X}}^{M} + \sum_{m=1}^{M} m d_{\mathcal{X}} \left(1 - P_{\text{out, }\mathcal{X}}\right) P_{\text{out, }\mathcal{X}}^{m-1}, \quad (13)$$

where $d_{\mathcal{X}}$ is the delay of a transmitted frame at the physical layer, which is computed from the instance that its burst is transmitted until its status is acknowledged. In particular, it can be calculated as

$$d_{\mathcal{X}} = \begin{cases} t_{\text{burst}} + \left\lceil \frac{2t_{\text{prop}}}{t_{\text{burst}}} \right\rceil t_{\text{burst}}, & \text{if } \mathcal{X} = \text{A}, \\ \ell_{\text{IL}} + \left\lceil \frac{2t_{\text{prop}}}{\ell_{\text{IL}}} \right\rceil \ell_{\text{IL}}, & \text{if } \mathcal{X} = \text{B}, \end{cases} \quad (14)$$

where t_{burst} is the burst transmission delay, and t_{prop} is the propagation delay. In here, we assume that (1) the receiver only processes once all the frames in a burst or the de-interleaver are received, and (2) the processing delay is negligible.

IV. Numerical Results & Discussions

This section presents and discusses the performance of four settings via theoretical analysis and simulations. The default parameters used for the results are as follows: propagation delay $t_{\text{prop}} = 2$ ms, burst transmission delay $t_{\text{burst}} = 1$ ms, symbol rate $R_{\text{s}} = 1$ GSps, interleaving time $\ell_{\text{IL}} = 5$ ms, and maximum number of ARQ rounds $M = 3$. Moreover, we consider the block interleaving as in [21], whose interleaver resolution is set as 8 bits. The evaluation is conducted on various datasets, each comprising one-second channel samples. Table I provides the physical characteristics of the considered datasets. Therein, scintillation index (SI) is used to quantify the effects of turbulence on the received optical signal, with a greater SI value corresponding to a stronger turbulence condition. The coherence time measures the time duration during which two recorded channel samples show high amplitude correlation. For the statistical behavior of each data set, we consider the well-known log-normal distribution. To assess the fitness between the experimental histogram data and

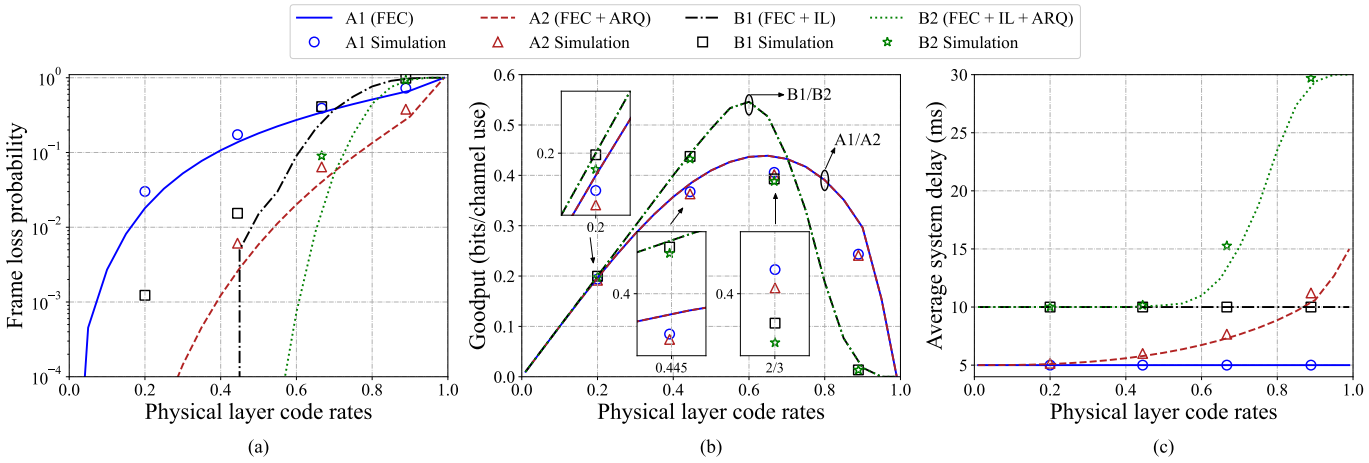

Fig. 3. (a) FLP, (b) goodput, and (c) average system delay of the considered settings versus the physical layer code rates (IL: interleaving).

the theoretical probability density function (PDF), we adopt the R^2 measure. Details on how to compute these physical characteristics can be found in [13], [22].

A. Impact and Selection of Physical Code Rate

First, we investigate the performance of all settings versus the physical layer code rate, as depicted in Fig. 3. The evaluation is conducted over the data set #2, and the average SNR is fixed at 7.5 dB. Moreover, Monte Carlo simulations are performed using the short Digital Video Broadcasting - Satellite - Second Generation (DVB-S2) low-density parity check (LDPC) codes [23]. The close agreement between the simulation and theoretical results confirms the accuracy and reliability of the proposed analytical framework. The results also reveal that the settings incorporating ARQ, which are A2 (- - -) and B2 (·····), achieve significantly lower FLP than those without ARQ, i.e., A1 (——) and B1 (-·-·). However, this gain comes with an increase in average system delay, mainly due to retransmission cycles required over the long-distance satellite link. Interestingly, the goodput performance remains identical between settings with and without ARQ. This is because the goodput measures the total successfully received data rate, irrespective of whether the data is delivered via initial transmissions or retransmissions. Based on these findings, it is recommended to enable ARQ in scenarios where minimizing FLP is a priority and when the system can tolerate a moderate increase in average delay. Conversely, in delay-sensitive applications, ARQ may be disabled to maintain lower latency, albeit at the expense of a higher FLP.

Another key observation is that the settings with interleaving, B1 (-·-·) and B2 (·····), deliver the best overall performance. This is due to interleaving's ability to disperse errors over multiple frames, mitigating deep fades and improving FEC efficiency. The trade-off, however, is increased average system delay, as deinterleaving requires all interleaved data to be received before decoding. Thus, interleaving is recommended when higher goodput and lower FLP are desired, provided delay constraints are flexible. Additionally, careful code rate selection is crucial to prevent performance degradation. For a given setting, an optimal code rate can be chosen to maximize the goodput while meeting a target FLP and delay threshold. For instance, with setting A2 (- - -), a physical layer code rate of 0.4 maximizes the goodput while retaining FLP below 10^{-3}.

B. Impact and Selection of Interleaving Times

Next, we investigate the proper selection of interleaving times. Fig. 4 presents the goodput and average system delay of setting B1 versus different interleaving times. As seen, the average frame delay increases when the interleaving time increases. The goodput, however, may either increase or decrease, depending on the selected code rate. For example, for $R_{\text{PHY}} = 0.7$ and $\overline{\gamma} = 5$ dB (—▲—), the goodput in all cases tends to decrease. This is because when the interleaving time increases, the ergodic capacity of each interleaving group in Eq. (9), $\mathcal{C}_{\text{erg}}^{(i)}$, will approach the overall ergodic capacity when considering all samples. It implies that the probability that the transmission rate when $R_{\text{PHY}} = 0.7$ is insufficient to support $\mathcal{C}_{\text{erg}}^{(i)}$ will increase. Therefore, the code rate should be carefully selected to avoid performance degradation. From the result, we can select the optimal interleaving time to maximize the goodput while minimizing the average frame delay. For instance, in Fig. 4(a), the interleaving time can be selected around 20 ms if $R_{\text{PHY}} = 0.5$ and $\overline{\gamma} = 5$ dB (—●—).

C. Investigation on Energy Efficiency

Another important issue is how different settings impact the energy aspect while maintaining the same performance. To assess this, we consider the required SNR per information bits for a specific setting to achieve a target level of FLP. This metric is computed as $E_b/N_0 = \frac{\overline{\gamma}_{\text{req}} \overline{m} \varkappa_d}{R_{\text{PHY}}}$, where $\overline{\gamma}_{\text{req}}$ is the required average SNR to reach the targeted FLP level, and can be computed numerically based on the information-theoretic framework in Section III. Fig. 5 presents the required SNR per information bits of all settings to achieve the FLP of 10^{-3}. It is observed that enabling ARQ and/or interleaving

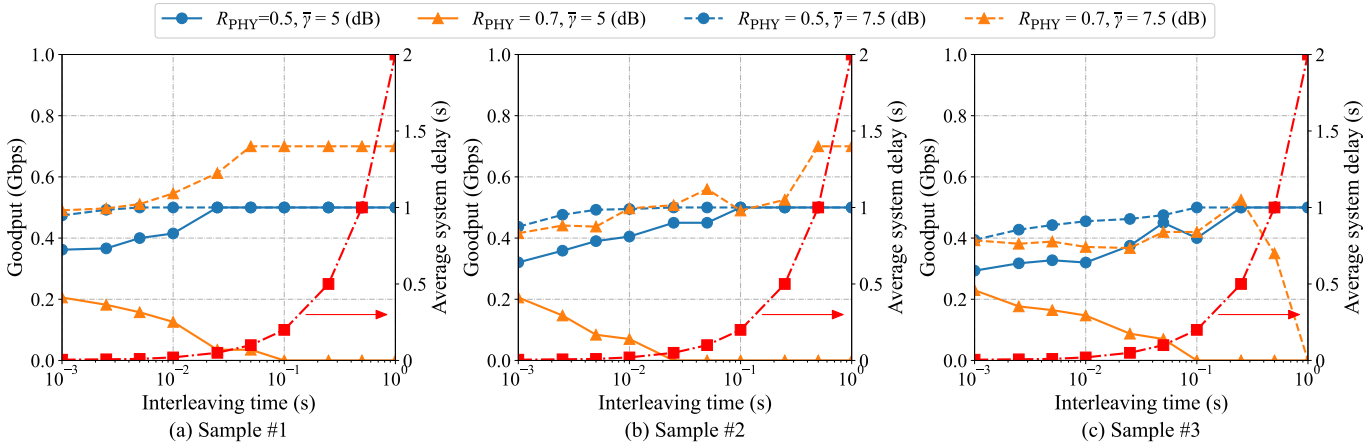

Fig. 4. Goodput and average system delay of system B1 (FEC + IL) versus different interleaving times.

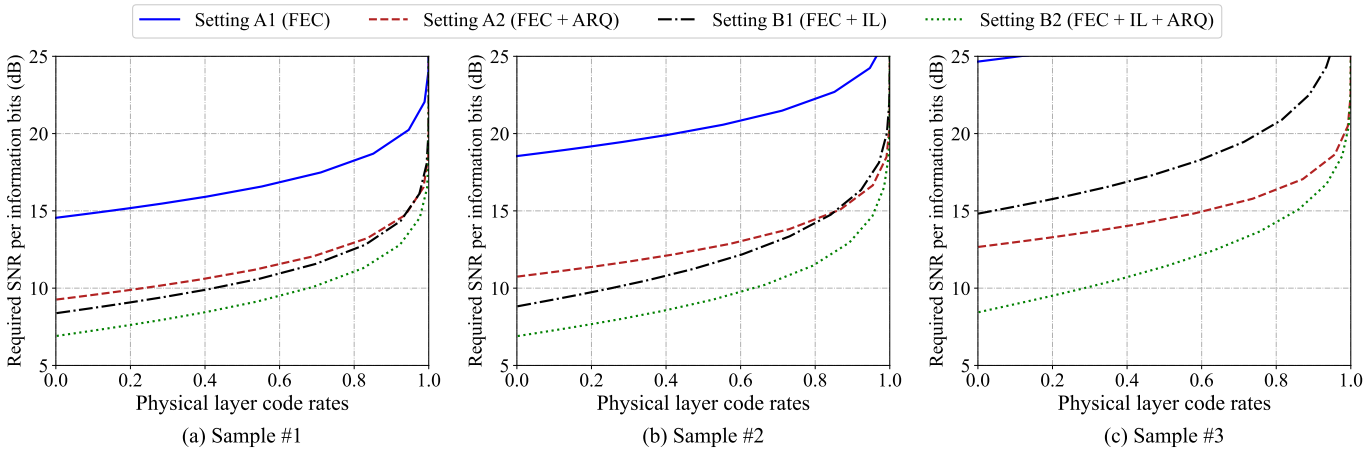

Fig. 5. The required SNR per information bits to achieve the FLP of 10^{-3}.

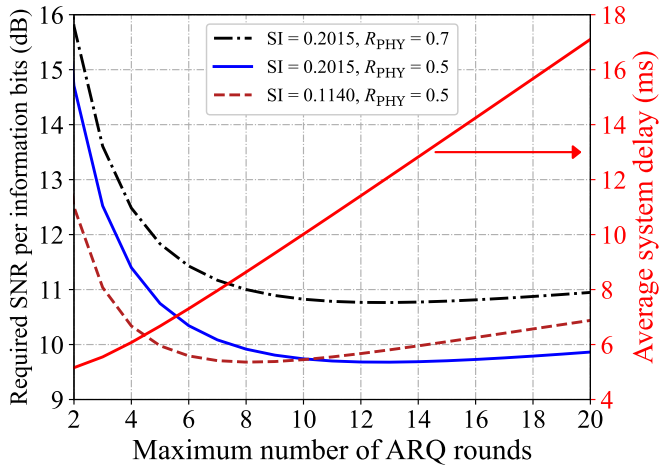

Fig. 6. The required SNR per information bits to achieve the FLP of 10^{-3}.

will improve FLP, implying that to achieve the same level of FLP, settings A2/B1/B2 will require a lower SNR compared to setting A1 (——). Moreover, it explains why setting A1 requires the highest SNR, while setting B2 (·····), combining both ARQ and interleaving, requires the lowest SNR among all settings. Another observation is that when the channel turbulence becomes stronger, setting A2 (- - -) gradually outperforms setting B1 (-·-·) over the range of considered code rates. This suggests that ARQ is a more robust option than interleaving in combating fading for applications requiring high energy efficiency.

Next, we investigate the effect of the maximum number of ARQ rounds M on the required SNR per information bits in Fig. 6. The results show that increasing M reduces the required SNR to maintain the same level of FLP. This is because a higher M allows us to relax on the outage probability of the physical layer, allowing the system to operate with less transmit power. This is especially important in maintaining reliability for energy-efficient satellite systems. For instance, when SI $= 0.2015$ and $R_{\text{PHY}} = 0.7$ (-·-·), the gain can be around 3 dB between $M = 3$ and $M = 8$.

However, setting the maximum number of ARQ rounds too high can lead to energy overconsumption due to repeated

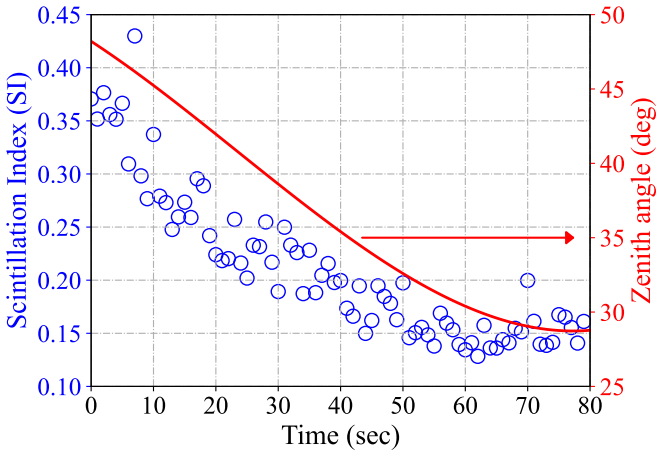

Fig. 7. SI and zenith angle over the considered satellite pass duration.

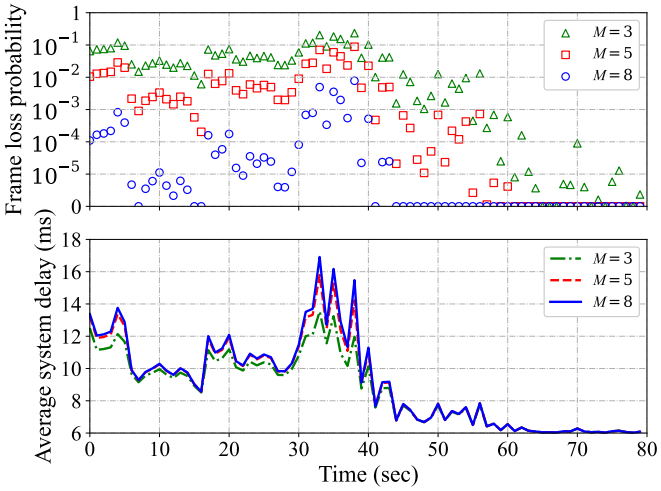

Fig. 8. Performance of setting A2 (FEC + ARQ) over the considered satellite pass duration with different maximum numbers of ARQ rounds, M.

retransmissions. This can be clearly observed in case SI $=$ 0.1140 and $R_{\text{PHY}} = 0.5$ (- - -), where the required level of SNR per information bit slightly increases when M surpasses 8. Moreover, another tradeoff is the increase in average system delay, as shown on the right axis. From the results, we can select the maximum number of ARQ rounds to maximize the energy efficiency while maintaining a level of average system delay. For instance, in the case that SI $= 0.2015$ and $R_{\text{PHY}} = 0.5$ (——), we can select the maximum number of ARQ rounds as $M = 10$ to maintain a target average system delay of 10 ms.

D. Performance Investigation Over A Satellite Pass

Next, we investigate the performance of the considered settings over a part of the satellite pass duration. The changing of SI and zenith angle over the considered duration are shown in Fig. 7. Each point of SI is calculated over one-second data of samples. Due to the change in zenith angle over the considered duration, we recalculate the propagation delay for each point

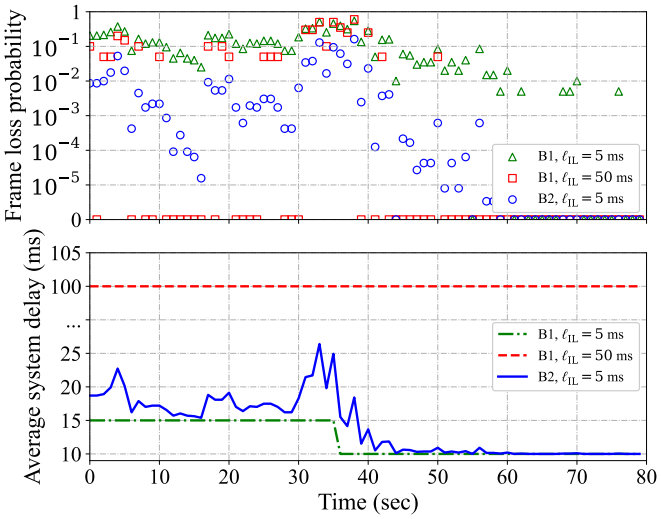

Fig. 9. Performance of setting B1 (FEC + IL) and B2 (FEC + IL + ARQ) over the considered satellite pass duration with ℓ_{IL}.

as $t_{\text{prop}} = \frac{H_{\text{sat}}}{\cos(\xi)c}$, where H_{sat} is the slant distance at 0-degree zenith angle and can be set as 600 km [12], ξ is the zenith angle, and c is the speed of light. The average SNR is set as 7.5 dB, and $R_{\text{PHY}} = 0.5$.

Fig. 8 presents the FLP and average system delay of setting A2 over the considered satellite pass duration with different maximum numbers of ARQ rounds, M. The results show that the FLP can be reduced when M increases with a negligible impact on the average system delay. This is because the transmitted frames barely reach the maximum number of ARQ rounds, and may be reliably delivered after a few ARQ rounds. Fig. 9 depicts the performance of setting B1 and B2 with different interleaving times. As shown, setting B1 with a 5-ms interleaver (△) is insufficient to guarantee system reliability. We can improve FLP by (1) increasing the interleaving time or (2) enabling the ARQ.

For the first option, setting B1 with $\ell_{\text{IL}} = 50$ ms (□) is investigated. It is shown that the interleaving groups either are error-free or experience a high loss. The FLP is highest during the period of $[30, 40]$ seconds. This may happen due to atmospheric disturbances, such as cloud coverage, which cause a degradation in the values of channel data samples. For the option that enables ARQ (○), the improvement in FLP is not as significant as when the interleaving time is increased to 50 ms. However, that option can retain the lowest FLP in the period of $[30, 40]$ seconds. Moreover, the increase in the system delay of setting B2 (——) is smaller than that of setting B1 with a longer interleaving time (- - -). These results highlight the potential of ARQ in ensuring the reliability of optical satellite communication systems.

E. LDPC Codes Performance

Finally, Fig. 10 describes the outage probability of two LDPC codes that are recommended for optical satellite systems, i.e., DVB-S2 and 5G New Radio (5G-NR) LDPC codes

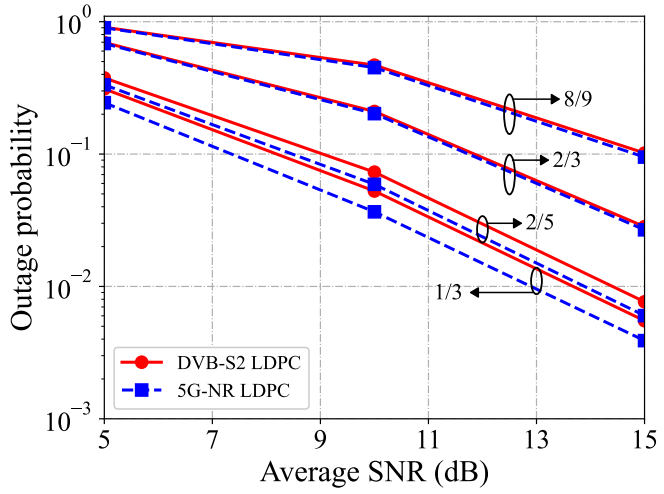

Fig. 10. FLP of DVB-S2 and 5G-NR LDPC codes for different code rates.

[3], [4]. The evaluation is conducted over the data set #2 with four code rates, i.e., $8/9, 2/3, 2/5$, and $1/3$. For DVB-S2 LDPC codes, all code rates have the same encoded block length, i.e., $kR_{\text{PHY}} = 16200$ bits [23]. As for 5G-NR LDPC codes, the parity check matrices of the considered rates are nested and have the same information length of $k = 8448$ bits [24]. Moreover, we utilize the sum-product decoding algorithm, in which the maximum number of iterations is set to 20. It is observed that the 5G-NR LDPC codes exhibit slightly better performance than the DVB-S2 LDPC codes at the rates of $2/5$ and $1/3$. It likely happens because 5G-NR LDPC codes have a longer encoded block length. Overall, both codes are powerful and good choices for optical satellite systems, each with different purposes.

V. Conclusion

This work presented a comparative analysis of different fade mitigation strategies for optical LEO-to-ground communication systems. Specifically, we developed an information-theoretic framework in terms of three link-layer performance metrics: FLP, goodput, and average system delay. The performance analysis also incorporated the recorded channel gain data from optical LEO-to-ground experiments. Importantly, the framework accounts for the finite interleaving time, offering a realistic and practical assessment of system behavior under varying operational conditions. From the numerical results, we discussed potential use cases and optimal parameter selection for each setting in different scenarios. We expect that the study can benefit the development and standardization of FSO-based satellite systems.

Acknowledgment

This work was supported by the Telecommunications Advancement Foundation (TAF) and the JSPS KAKENHI Grant number 24K14918.

References

[1] D. R. Kolev *et al.*, "Latest developments in the field of optical communications for small satellites and beyond," *J. Lightwave Technol.*, vol. 41, no. 12, pp. 3750–3757, Jun. 2023.
[2] CCSDS, "Optical communications physical layer," CCSDS 141.0-B-1, Tech. Rep., 2019.
[3] ——, "Optical high data rate (HDR) communication-1550 NM," CCSDS 141.0-O-1, Tech. Rep., 2022.
[4] S. D. Agency, "Optical communications terminal (OCT) standard version 3.1.0." Space Development Agency, Tech. Rep., 2023.
[5] Y. Yamashita, E. Okamoto, Y. Iwanami, Y. Shoji, M. Toyoshima, and Y. Takayama, "A markov-based satellite-to-ground optical channel model and its effective coding scheme," *IEICE Trans. Commun.*, vol. 95, no. 1, pp. 254–262, Jan. 2012.
[6] H. Inoue, E. Okamoto, Y. Shoji, Y. Takayama, and M. Toyoshima, "Comparative study on low-rate forward error correction codes in downlink satellite-to-ground laser communications," *Proc. IEEE Int. Conf. Space Opt. Syst. Appl. (ICSOS)*, 2014.
[7] H. Takenaka *et al.*, "Study on coding parameters for a small optical transponder," *Proc. IEEE Int. Conf. Space Opt. Syst. Appl. (ICSOS)*, 2014.
[8] S. Poulenard *et al.*, "Forward error correcting code for high data rate LEO satellite optical downlinks," in *Proc. IEEE Int. Conf. Space Opt. (ICSO)*, vol. 11180, 2019, pp. 2029–2038.
[9] D. T. Nguyen and Y. Park, "Performance analysis of interleaved LDPC for optical satellite communications," *Opt. Commun.*, vol. 442, pp. 13–18, Jul. 2019.
[10] N. Mazzali and P.-D. Arapoglou, "Channel interleaver dimensioning for optical LEO direct-to-earth systems," in *Proc. 10th Adv. Satell. Multimedia Syst. Conf. 16th Signal Process. Space Commun. Workshop*, 2020, pp. 1–6.
[11] C. M. Schieler *et al.*, "Recent on-orbit results and ARQ performance analysis for the TBIRD 200-Gbps mission," in *Proc. IEEE Int. Conf. Space Opt. Syst. Appl. (ICSOS)*, 2023, pp. 49–55.
[12] D. R. Kolev and M. Toyoshima, "Satellite-to-ground optical communications using small optical transponder (SOTA)–received-power fluctuations," *Opt. Express*, vol. 25, no. 23, pp. 28 319–28 329, 2017.
[13] ——, "Received-power fluctuation analysis for LEO satellite-to-ground laser links," *J. Light. Technol.*, vol. 35, no. 1, pp. 103–112, Jan. 2017.
[14] A. A. Farid and S. Hranilovic, "Outage capacity optimization for free-space optical links with pointing errors," *J. Lightwave Technol.*, vol. 25, no. 7, pp. 1702–1710, Jul. 2007.
[15] F. Yang, J. Cheng, and T. A. Tsiftsis, "Free-space optical communication with nonzero boresight pointing errors," *IEEE Trans. Commun.*, vol. 62, no. 2, pp. 713–725, Feb. 2014.
[16] S. M. Aghajanzadeh and M. Uysal, "Information theoretic analysis of hybrid-ARQ protocols in coherent free-space optical systems," *IEEE Trans. Commun.*, vol. 60, no. 5, pp. 1432–1442, May 2012.
[17] E. Zedini, A. Chelli, and M.-S. Alouini, "Unified performance analysis of hybrid-ARQ with incremental redundancy over free-space optical channels," in *Proc. IEEE Int. Symp. Pers. Ind. Mobile Radio Commun. (PIMRC)*, Sept. 2014, pp. 774–778.
[18] R. L. Burden and J. D. Faires, *Numerical methods*, 9th ed. Boston, MA, USA: Cengage Learning, 2010.
[19] J. Li and M. Uysal, "Optical wireless communications: system model, capacity and coding," in *Proc. IEEE 58th Veh. Technol. Conf.*, vol. 1, Oct. 2003, pp. 168–172.
[20] Y. Chang, S. Cai, L. Wang, H. Zhang, and Z. Zhang, "Experimental analysis of reducing outage probability using deep interleaving for long-distance free space optical systems," *IET Optoelectronics*, vol. 18, no. 4, pp. 121–129, Jul. 2024.
[21] D. R. Arrieta *et al.*, "Proof-of-concept real-time implementation of interleavers for optical satellite links," *J. Lightwave Technol.*, vol. 41, no. 12, pp. 3932–3942, May 2023.
[22] J. A. Anguita, M. A. Neifeld, B. Hildner, and B. Vasic, "Rateless coding on experimental temporally correlated FSO channels," *J. Lightwave Technol.*, vol. 28, no. 7, pp. 990–1002, Apr. 2010.
[23] *Digital video broadcasting (DVB); second generation framing structure, channel coding and modulation systems for broadcasting, interactive services, news gathering and other broadband satellite applications*, ETSI EN 302-307 v1.1.1, 2014.
[24] *Multiplexing and Channel Coding (Release 15)*, document TS 38.212 V15.1.1, 3GPP, Apr. 2018.